CONF-8410142--72

BWR Pipe Crack and Weld Clad Overlay Studies*

by

W. J. Shack, T. F. Kassner, P. S. Maiya,
J. Y. Park, and W. E. Ruther

CONF-8410142--72

TI85 004067

ARGONNE NATIONAL LABORATORY
9700 South Cass Avenue
Argonne, Illinois 60439

Materials Science and Technology Division

October 1984

DISCLAIMER

To be presented at the 12th Water Reactor Safety Research Information Meeting, October 22-26, 1984, sponsored by the U.S. Nuclear Regulatory Commission, Washington, D. C.

*Work supported by the U.S. Nuclear Regulatory Commission.

BWR Pipe Crack and Weld Clad Overlay Studies*

by

W. J. Shack, T. F. Kassner, P. S. Maiya,
J. Y. Park and W. E. Ruther

Materials Science and Technology Division
ARGONNE NATIONAL LABORATORY
Argonne, Illinois 60439

Leaks and cracks in the heat-affected zones of weldments in austenitic stainless steel piping in boiling water reactors (BWRs) due to intergranular stress corrosion cracking (IGSCC) have been observed since the mid-1960s. Since that time, cracking has continued to occur, and indications have been found in all parts of the recirculation system, including the largest diameter lines.

Proposed solutions for the problem include procedures that produce a more favorable residual stress state on the inner surface, materials that are more resistant to stress corrosion cracking (SCC), and changes in the reactor environment that decrease the susceptibility to cracking. In addition to the evaluation of these remedies, it is also important to gain a better understanding of the weld overlay procedure, which is the most widely used short-term repair for flawed piping.

TECHNICAL PROGRESS

The main areas of effort during the past year have been (1) studies of the effects of impurities, dissolved oxygen content, and strain rate on susceptibility to SCC in "Nuclear Grade" Type 316NG and sensitized Type 304 stainless steel, (2) finite-element analyses and experimental measurement of residual stresses in weldments with weld overlays, and (3) analysis of field components to assess effectiveness of in-service inspection techniques and the in-reactor performance of weld overlay repairs. Work at ANL on acoustic leak detection and nondestructive evaluation is reported elsewhere in these Proceedings by D. S. Kupperman et al.[1]

Effects of Impurities and Dissolved Oxygen on the IGSCC Susceptibility of Sensitized Stainless Steels

In addition to dissolved oxygen produced by radiolytic decomposition of the water and corrosion products, other impurity species can enter the coolant through a number of sources (condensate and reactor-water cleanup demineralizers, the condensate storage tank, the suppression pool and reactor heat removal system, etc.). Demineralizer systems on BWRs remove contaminants introduced by condenser in-leakage and unanticipated upsets in water chemistry. However, demineralizer resins are also a source of contamination owing to the leakage of ion-exchange resin fragments to the system during normal operation and to the release of ions to the coolant after regeneration of the resins.

The high temperature and neutron flux in the reactor core cause rapid decomposition of resin fragments that enter the recirculation water. A number

of anion species can be introduced by resin ingress and decomposition (e.g., SO_4^{2-}, NH_3-NH_4^+, NO_2^-, and NO_3^-, as well as by ion exchange (e.g., Cl^-, CO_3^{2-}, and PO_4^{3-}.

The relative effect of these anions, in conjunction with hydrogen and sodium cations (i.e., under slightly acidic or basic conditions, respectively), on the SCC susceptibility of lightly sensitized Type 304 SS has been evaluated in constant-extension-rate (CERT) tests. Anion concentrations in these tests were set at 0.1 ppm. However, the actual concentration of the species will depend on dissociation equilibria at high temperature. These concentrations gave conductivity values of $\leq$1 μS/cm. The effect of the different anions with sodium on the time to failure is shown in Fig. 1. Ductile plus transgranular failures occurred in high-purity water and in water containing nitrate and borate; only a small decrease in the time to failure resulted from the addition of these ions. The other anions were more deleterious. The effects of carbonate and chloride were virtually identical. Phosphate and silicate produced a somewhat greater degree of IGSCC. The sulfur species (viz., sulfate, sulfite, thiosulfate, and sulfide) were the most deleterious.

Added as acids, silicate, borate, nitrate, and phosphate produced the smallest change in CERT parameters; carbonate and chloride were somewhat more deleterious and the sulfur species caused the higheat degree of IGSCC. The time-to-failure results shown in Fig. 2 are consistent with those obtained for other CERT parameters.

Comparison of the results for the dilute acids with those for the sodium salts indicates that nitrate, borate, carbonate, and chloride are somewhat more deleterious when added in acid form; however, there is essentially no difference for the sulfur species.

Since the various anion species differ considerably in their effect on IGSCC susceptibility, it is unlikely that susceptibility to cracking can be correlated with conductivity and pH without a knowledge of the specific ions present. The standard instrumentation for routine analyses of reactor coolant is, in general, not adequate to detect the sulfur species that are particularly deleterious from the standpoint of IGSCC even though sulfate is likely to be present in BWR water at low concentrations ($\leq$0.1 ppm) from normal resin leakage and from resin regeneration and replacement operations.

Although CERT tests are very useful for studying the effects of impurities on SCC susceptibility, the severe mechanical loading produced during the tests makes it difficult to use the results quantitatively. Therefore, fracture-mechanics crack-growth-rate type tests are being performed to supplement the CERT tests. Because of the long times required for these tests, only a limited range of conditions can be considered.

Baseline tests were performed in high-purity water with 8 ppm dissolved oxygen at 289°C. Three 1TCT specimens were stressed at a load ratio of 0.95 and an initial maximum stress intensity K_{max} of 28 MPa $m^{\frac{1}{2}}$ under a positive sawtooth waveform. As expected, the most heavily sensitized material had the highest crack growth rate. The crack growth rate increased by about an order of magnitude as the cyclic frequency was increased from $\sim 10^{-2}$ to $\sim 10^{-1}$ Hz. For this heat of material and these test conditions, crack growth rates appear to be

sensitive to small superposed cyclic loading, although the measured crack growth rates are within the scatter band obtained for a number of heats of material under constant loading conditions.[3]

After baseline tests were completed, the effect of dissolved oxygen concentration was evaluated. The dissolved oxygen level was maintained at ~0.2 ppm for ~1000 h, decreased to 0.02 ppm for ~600 h, and then increased back to 0.2 ppm. The crack length as a function of time is shown in Fig. 3. Crack growth virtually ceased over the ~600-h time interval at the low dissolved oxygen concentration. It resumed at approximately the initial rates after the dissolved oxygen concentration was increased to the 0.2 ppm value.

The crack growth rate for the more heavily sensitized material (EPR = 20 C/cm^2) in water with 0.2 ppm dissolved oxygen is approximately half of that obtained in water with 8 ppm dissolved oxygen, as expected. Surprisingly, the crack growth rate of the lightly sensitized material (EPR = 2 C/cm^2) is approximately an order of magnitude higher at the lower dissolved oxygen concentrations. Measurable crack growth rates were also observed in the solution-annealed specimen. It appears that once a sharp crack (or tight crevice) is introduced (by fatigue precracking in this instance), propagation can occur under conditions that would not normally be considered to lead to environmentally-assisted cracking.

Fractographic examination of the specimens showed that the crack mode was primarily intergranular in the sensitized specimens and transgranular in the solution-annealed specimen. However, the decrease in crack growth rate in the solution-annealed specimen when the oxygen was decreased indicates that even the transgranular growth is strongly influenced by the environment.

A similar crack growth experiment was performed to investigate the effect of an impurity, 0.1 ppm sulfate (as H_2SO_4), on the crack growth rate. After ~6000 h of testing, the sulfate level in the feedwater was reduced to a very low level for a period of ~1200 h. After this time interval, the sulfate level was again increased to 0.1 ppm.

The crack lengths as a function of time for this portion of the test are shown in Fig. 4. Stress intensity values for the lightly sensitized specimen (EPR = 2 C/cm^2) at different times are noted on the figure. Removal of the sulfate had virtually no effect on crack growth in the solution-annealed and the more heavily sensitized (EPR = 20 C/cm^2) specimens. The crack growth rate of the lightly sensitized specimen decreased by a factor of ~4 over an ~600-h period after sulfate was removed from the feedwater; however, the rate in high-purity water increased over the next 600 h to the initial value observed in the water with 0.1 ppm sulfate. A further increase in the crack growth rate occurred at ~7300 h when sulfate was again added to the feedwater. Roughly half of this increase in crack growth rate can be attributed to the increase in stress intensity factor due to the growth of the crack. If we assume that the initial decrease in the crack growth rate was due to a change in crack tip chemistry associated with the removal of sulfate from the bulk water, it is possible that sulfate or other sulfur species slowly desorbed from the oxide films, migrated to the crack tip zone, and subsequently accelerated the crack growth process.

The effects of the dissolved oxygen and the sulfate additions observed in the fracture-mechanics crack-growth-rate tests are qualitatively consistent with the crack growth information obtained from CERT tests on the same heat of material.[4] However, reduction of the dissolved oxygen to very low levels causes a much larger relative reduction in crack growth rates in the fracture-mechanics crack-growth-rate tests than in the corresponding CERT tests.[4]

Effects of Impurities on the SCC Susceptibility of Type 316NG Stainless Steel

Our previous work has shown that Type 316NG stainless steel can crack transgranularly in oxygenated water (0.2 ppm O_2) with impurities (0.1 ppm sulfate, added as acid).[3] Additional work has[2] shown that in CERT tests in the strain-rate regime 10^{-6} to 10^{-7} s^{-1}, cracking occurs only when impurities are present. Since an environment containing 0.1 ppm sulfate (added as acid) represents the maximum impurity level currently permitted under normal operating conditions, it is essential to know whether transgranular cracking in Type 316NG stainless steel can occur at lower levels of impurities. Test results for various sulfate impurity concentrations (<0.1 ppm) and strain rates are summarized in Table 1 together with previously reported data. At a strain rate $\dot{\varepsilon} = 1 \times 10^{-6}$ s^{-1}, cracking occurs only when the sulfate level is >0.075 ppm, which suggests that the critical impurity concentration for transgranular cracking at this strain rate is ~0.1 ppm sulfate. When the strain rate is lowered to 2×10^{-7} s^{-1}, cracking occurs at even lower sulfate concentrations (0.05 ppm). However, the average crack growth rate $\dot{a}_{av}$ decreases by a factor of ~3 compared to that determined in an environment with 0.1 ppm sulfate.

These results suggest that the critical level of impurity concentration need to produce transgranular cracking decreases with a decrease in strain rate. In conjunction with the complete absence of TGSCC in high-purity water at $\dot{\varepsilon} = 10^{-6}$ to 10^{-7} s^{-1}, they confirm that transgranular cracking in Type 316NG stainless steel is directly related to the impurity level and suggest that significant benefits can be achieved by close control of the coolant chemistry.

Effect of Strain Rate on SCC Susceptibility

A phenomenological model for SCC susceptibility that describes the effects of the applied strain rate $\dot{\varepsilon}$ on SCC has been developed.[6] The model gives simple power-law correlations between $\dot{\varepsilon}$ and parameters such as $\dot{a}_{av}$ and time to failure and is based on an estimate of the crack-tip strain obtained by use of a J-integral approach, the slip-dissolution model of Ford,[7] and a J-integral fracture criterion. The correlations between the SCC susceptibility parameters and the strain rate are of the form

$$\varepsilon_f = (J_c/AC)^{2/3} \dot{\varepsilon}^{1/3} , \quad (1)$$

$$a_f = A(J_c/AC)^{1/3} \dot{\varepsilon}^{-1/3} , \quad (2)$$

$$t_f = (J_c/AC)^{2/3} \dot{\varepsilon}^{-2/3} , \text{ and} \quad (3)$$

$$\dot{a}_{av} = A(AC/J_c)^{1/3} \dot{\varepsilon}^{1/3} , \quad (4)$$

where ε_f, a_f, and t_f are the strain, crack length, and time at failure; $\dot{a}_{av}$ is the average crack growth rate; and A, J_c, and C are constants which depend on the material and environment.

Good agreement is obtained between the results of the analysis and CERT results over a fairly wide range of strain rates, as shown in Figs. 5 and 6.

Analysis of Field Components with Weld Overlays

Laboratory ultrasonic examination, dye penetrant examination, residual stress measurements, metallographic examination, and sensitization measurements were performed on two 12-in.-diameter Type 304 stainless steel pipe-to-elbow weldments (Weld Nos. 2B31-1RC-12BR-C2 and -C3) removed from the primary coolant recirculation piping of the Hatch-2 boiling water reactor (BWR). Overlays were applied to these weldments after ultrasonic in-service inspection (ISI) had indicated cracking. After about one additional year of service, the recirculation piping in Hatch-2 was replaced and the weldments were removed for examination. The weldments were electrochemically polished by Quadrex Inc. to remove corrosion film and reduce radiation levels.

During the original ultrasonic ISI, intermittent indications around the entire circumference on the pipe side were reported for both weldments. The crack depths were estimated to be 28% throughwall for Weld No. 2B31-1RC-12BR-C2 and 30% for Weld No. -C3. However, little correlation was observed between the ISI results and the results of the dye penetrant tests and destructive examinations at ANL. Twenty short penetrant testing (PT) indications were observed on weldment C2 (fifteen on the elbow side and five on the pipe side). The indications were of a variety of types (axial, circumferential, skewed, or point), and most of them were located within 8 mm of the weld fusion lines (WFLs). There were no undercuts at the WFLs that produced PT indications in either weldment. No PT indications were observed on weldment C3. Even after sections from weldment C3 were subjected to three-point bending in order to open tight cracks that might be present, PT again indicated no cracks.

Before destructive examination, blind and partially blind ultrasonic tests (UTs) were carried out. Comparison of the UT results with the results of the PT and the metallographic sectioning indicates that the detection of cracks through the overlay by UT is difficult and at present unreliable.

The weldments were sectioned at a number of selected locations. The cross sections were metallographically polished and examined for cracks, defects, or any other features that might produce UT or PT indications. There was no evidence anywhere on the entire inner surface of the weldments that the counterbore was the cause of the cracking, although some details of the features on the inner surface may have been removed by electrochemical polishing at Quadrex.

The sectioning showed that the circumferential PT indications and the point PT indication were associated with short (<20 mm) circumferential intergranular cracks, and that the axial PT indication was associated with an axial intergranular crack. The depths of the circumferential cracks were 2-13 mm.

The crack profile of the 13-mm-deep (57% throughwall including the overlay) axial crack is shown in Fig. 7. In the interior of the pipe wall, the crack extended about 17 mm from the WFL, which is much further than suggested by the PT indication (1.5 mm long) at the inner surface of the weldment. The profile is somewhat unusual in shape. The crack tip was blunted, as shown in Fig. 8. Blunting of crack tips by weld overlays is predicted by finite-element analyses and would be expected to inhibit further crack growth. There was no evidence of tearing or extension of the crack beyond the blunted region. Metallographic sections were also obtained at a number of positions that produced strong UT signals but showed no PT indications. No cracks or discernible metallographic features (weld defects, inclusions, etc.) or geometrical irregularities were observed.

Experimental Measurement of Residual Stresses Produced by Weld Overlays

Measurements of surface and throughwall residual stresses have been made on three mock-up weldments supplied by Georgia Power and NUTECH for analysis. The weldments were fabricated 12-in. Schedule 100 pipe. One side of each weldment had a long, smooth weld prep geometry typical of that used in the Hatch-1 reactor, while the other side of each weldment had a short weld prep geometry typical of that used in the Hatch-2 reactor. Weld overlays were applied to two of the mock-up weldments after the weldments were fabricated by conventional butt welding procedures. The third weldment was fabricated by Last-Pass-Heat-Sink-Welding (LPHSW).

The two overlays are similar to those actually applied to the recirculation piping in the Hatch-2 reactor and were prepared with identical procedures, but they are slightly different in size. One (the "minioverlay") is ∿100 mm long and ∿5 mm thick. The other (the "standard" overlay) is ∿125 mm long and ∿5 mm thick.

As shown in Figs. 9 and 10, both the overlay procedures and LPHSW were very successful in inducing compressive residual stresses on the inner surfaces of the weldments for both weld prep geometries. The measured results are in general agreement with finite-element predictions supplied by NUTECH and E. F. Rybicki, Inc.

The residual stresses for the LPHSW mock-up are similar to those for the minioverlay and the standard overlay, at least for the region near the weld. On the basis of this set of weldments, differences in the stresses produced by the different procedures are small and appear to be within the range of variations that might be expected from weld to weld with a single procedure. The overlay procedures probably produce larger plastic strains and deformations, but since the stress is a relatively weak function of strain during plastic deformation, the corresponding stresses produced by the different procedures do not differ too greatly.

In Figs. 11-13, the throughwall axial residual stresses ∿2 mm from the WFLs are shown for the LPHSW weldment and the overlays. The depth shown in the figures is nondimensionalized with respect to the total thickness, i.e., wall plus overlay. As expected, the stresses are strongly compressive on the inner portion of the wall and tensile on the outer portion. These distributions should not be interpreted to indicate that the overlay will be effective for

cracks roughly halfway through the wall and ineffective for deeper cracks, since finite-element results[8] show that the presence of a crack strongly perturbs the stresses produced by the overlay process. Although these results do confirm the analytical predictions of strongly compressive stress fields produced on the inner surface by the overlay, other types of tests are needed to verify the predicted stress fields at crack tips.

FUTURE WORK

Work to assess the effect of impurities on SCC in both conventional BWR environments and the low-oxygen environment characteristic of BWRs with hydrogen additions will continue. The emphasis will be on the effect of low levels of impurities well within current water chemistry guidelines. The effects of impurities on crack growth rates in Type 308 weld metal will be examined. The effect of chemistry transients will also be examined further with fracture-mechanics crack-growth-rate tests. Low-stress cyclic pipe tests will be carried out to assess the effect of impurities under more prototypic loading conditions. The effectiveness of low oxygen levels in inhibiting SCC in irradiated materials will be examined. Long-term aging studies on Types 316NG and 304 stainless steel will also continue.

REFERENCES

1. D. S. Kupperman, T. N. Claytor, D. W. Prine, and T. A. Mathieson, Evaluation of Methods for Leak Detection in Reactor Primary Systems and NDE of Cast Stainless Steel, these Proceedings.

2. R J. Kurtz, D. W. Shannon, B. Francis, F. M. Kustas, and P. L. Koelmstedt, Evaluation of BWR Resin Intrusions on Stress Corrosion Cracking of Reactor Structural Materials, EPRI Final Report, NP-3145, Electric Power Research Institute (June 1983).

3. R. Horn et al., The Growth and Stability of Stress Corrosion Cracks in Large-Diameter BWR Piping, EPRI NP-2472, Vol. 2, Electric Power Research Institute (July 1982).

4. W. E. Ruther, W. K. Soppet, and T. F. Kassner, in Environmentally Assisted Cracking in Light Water Reactors: Annual Report, October 1982-September 1983, NUREG/CR-3806, ANL-84-36, Argonne National Laboratory (June 1984), pp. 101-124.

5. P. S. Maiya and W. J. Shack in Environmentally Assisted Cracking in Light Water Reactors: Annual Report, October 1982-September 1983, NUREG/CR-3806, ANL-84-36 (June 1984), pp. 62-75.

6. P. S. Maiya and W. J. Shack, "Effects of Nominal and Crack-tip Strain Rate on IGSCC Susceptibility in CERT Tests," in Embrittlement by the Localized Crack Environments, R. P. Gangloff, ed., The Metallurgical Society of AIME, Warrendale, PA (1984), pp. 199-209.

7. F. P. Ford, "Mechanisms of Stress Corrosion Cracking," in Aspects of Fracture Mechanics in Pressure Vessels and Piping, PVP-Vol. 58, ASME, New York (1982), pp. 229-269.

8. P. S. Maiya and W. J. Shack, in Environmentally Assisted Cracking in Light Water Reactors: Annual Report, October 1982-September 1983, NUREG/CR-3806, ANL-84-36, Argonne National Laboratory (June 1984), pp. 83-92.

Table 1. CERT Test Results for Type 316NG SS (Heat P91576, 1050°C/0.5 h + 650°C/24 h) in Oxygenated Water (0.2 ppm O_2) with SO_4^{2-} Impurity. T = 289°C, ε_o = 1.0%, and a_o = 1 μm.

Test Number	$\dot{\varepsilon}$, s^{-1}	SO_4^{2-}, ppm	Conductivity, μS/cm	t_f, h	σ_{max}, MPa	Failure Mode	$\dot{a}_{av}$, m/s
157	1×10^{-5}	0.1	0.9	9.7	430	Ductile	-
159	2×10^{-6}	0.1	0.9	53.5	453	Ductile	-
186	1×10^{-6}	0.0	~0.1	100.3	457	Ductile	-
206	1×10^{-6}	0.01	0.13	100.6	447	Ductile	-
202	1×10^{-6}	0.05	0.47	123.0	450	Ductile	-
214	1×10^{-6}	0.075	0.72	107.6	438	Ductile	-
160	1×10^{-6}	0.10	0.9	100.6	450	TGSCC	1.51×10^{-9}
154[a]	1×10^{-6}	0.10	0.9	109.4	458	TGSCC	1.50×10^{-9}
169	4×10^{-7}	0.10	0.9	217.4	462	TGSCC	9.74×10^{-10}
207	2×10^{-7}	0.01	0.13	497.3	468	Ductile	-
199	2×10^{-7}	0.05	0.47	588.7	449	TGSCC	2.21×10^{-10}
172	2×10^{-7}	0.10	0.90	474.0	461	TGSCC	7.35×10^{-10}
148	9.5×10^{-8}	0.1	0.9	565.9	472	TGSCC	6.73×10^{-10}

[a] 8 ppm O_2.

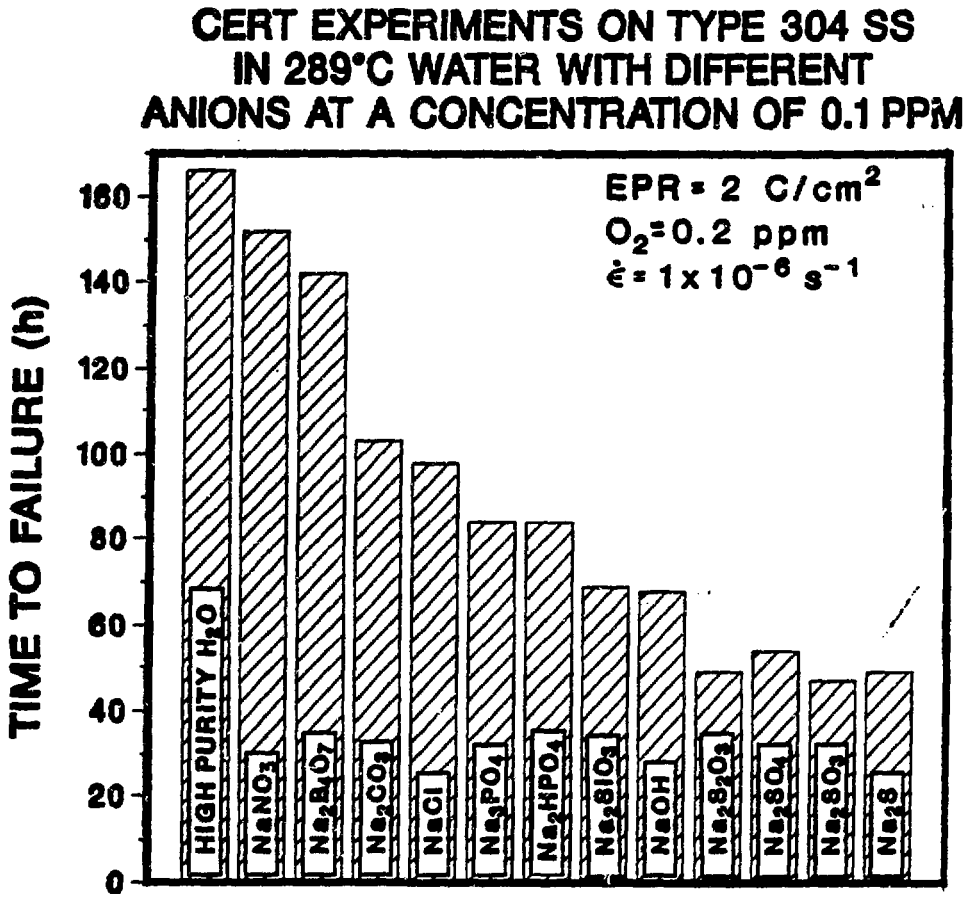

Fig. 1. Effect of Various Sodium Salts at an Anion Concentration of 0.1 ppm in Water Containing 0.2 ppm Dissolved Oxygen on the Time to Failure of Lightly Sensitized Type 304 SS Specimens in CERT Experiments at 289°C and a Strain Rate of 1×10^{-6} s^{-1}.

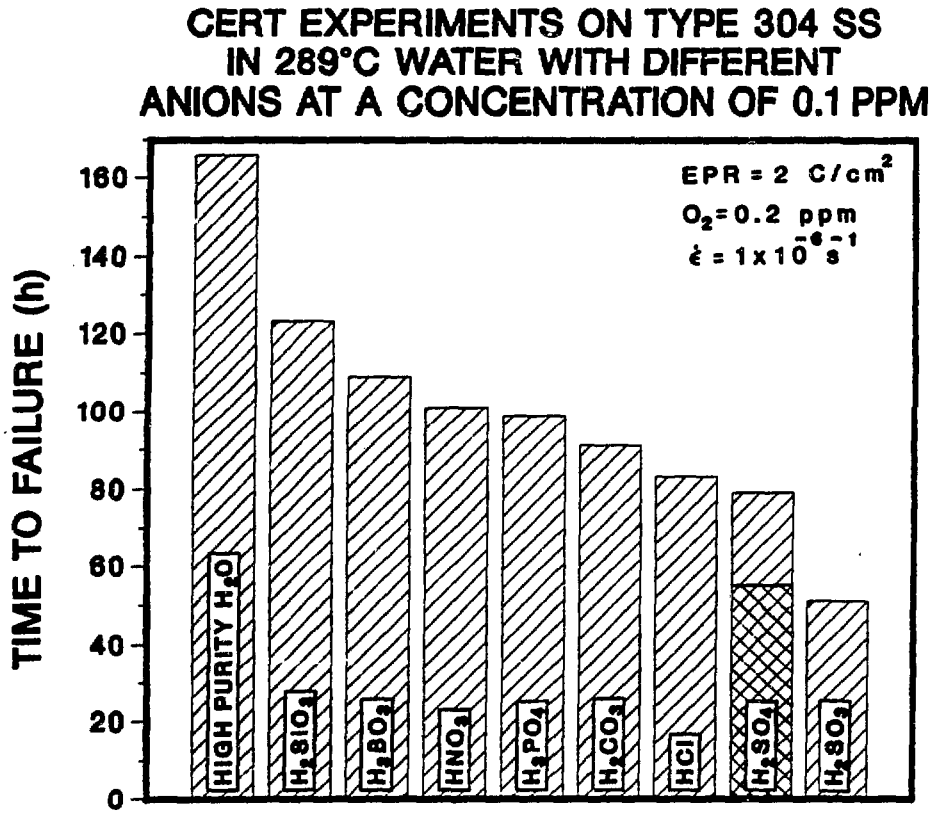

Fig. 2. Influence of Various Acids at an Anion Concentration of 0.1 ppm, in Water Containing 0.2 ppm Dissolved Oxygen, on the Time to Failure of Lightly Sensitized Type 304 SS Specimens in CERT Experiments at 289°C and a Strain Rate of 1×10^{-6} s^{-1}. Two tests were run with H_2SO_4.

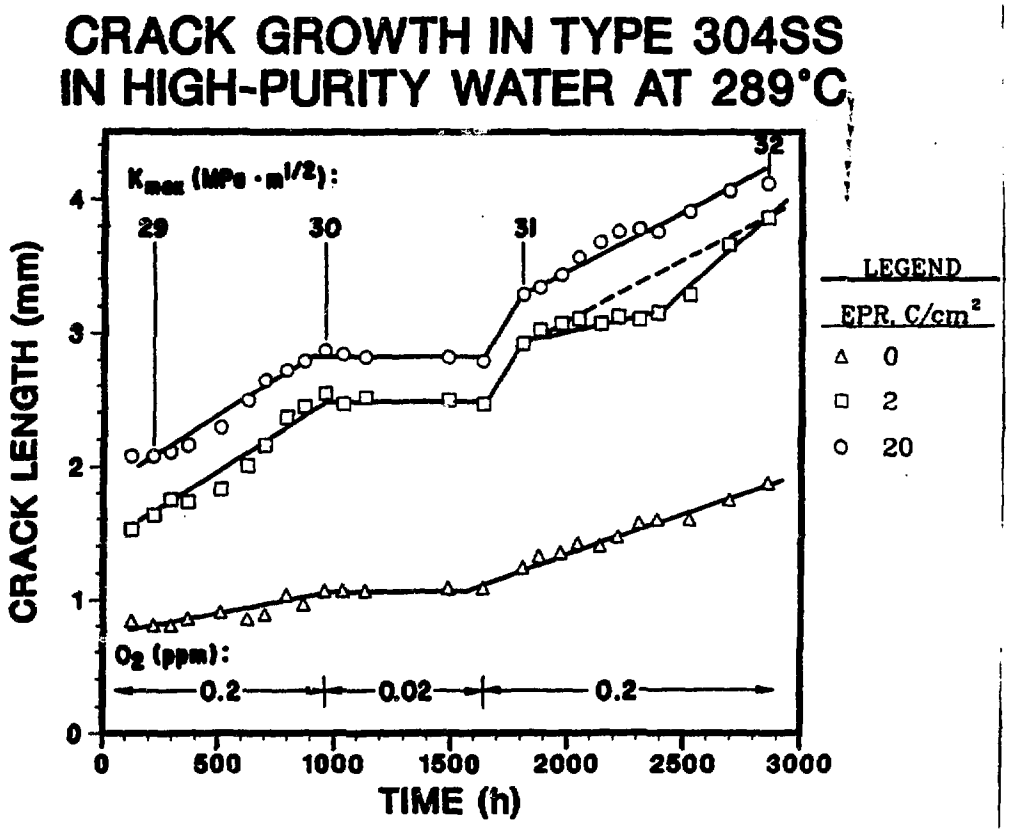

Fig. 3. Crack Length versus Time for 1TCT Specimens of Solution-annealed (EPR = 0) and Sensitized (EPR = 2 and 20 C/cm^2) Type 304 SS in 289°C Water Containing 0.2 ppm Dissolved Oxygen, Except for an Intermediate Period in Which the Oxygen Concentration was Decreased to 0.02 ppm. The loading conditions for the positive sawtooth waveform with a slow loading time (12 s) and a rapid unloading (1 s) are as follows: load ratio R = 0.95, frequency = 8 x 10^{-2} Hz, and K_{max} = 29 to 32 MPa·m$^{\frac{1}{2}}$ for the specimen with the largest crack.

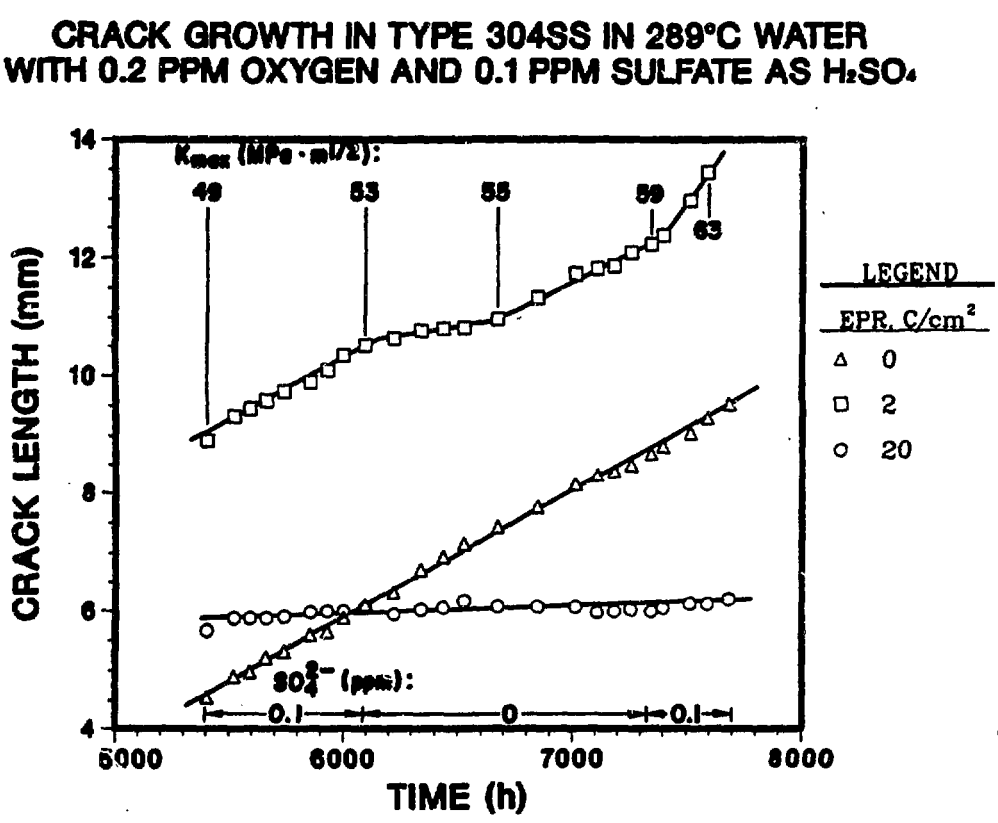

Fig. 4. Crack Length versus Time for 1TCT Specimens of Solution-annealed (EPR = 0) and Sensitized (EPR = 2 and 20 C/cm^2) Type 304 SS in 289°C Water Containing 0.2 ppm Dissolved Oxygen and 0.1 ppm Sulfate as H_2SO_4, Except for an Intermediate Period with High-Purity Water. The loading conditions for the positive sawtooth waveform with a slow loading time (12 s) and a rapid unloading (1 s) are as follows: load ratio R = 0.95, frequency = 8×10^{-2} Hz, and K_{max} = 49 to 63 MPa·m$^{\frac{1}{2}}$ for the specimen with the largest crack.

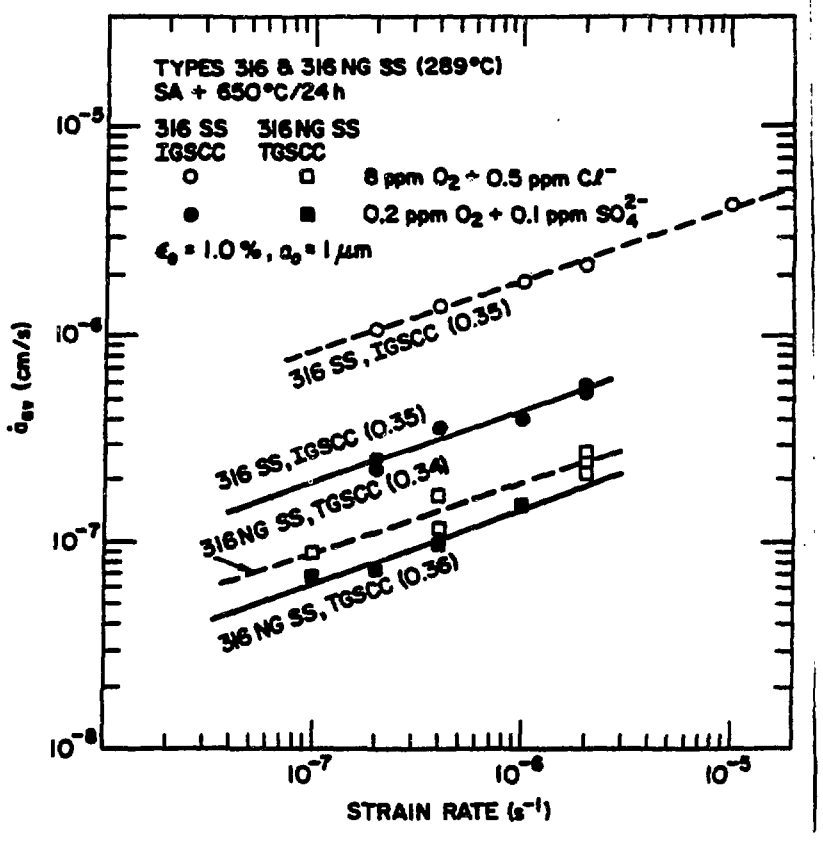

Fig. 5. Correlation between Average Stress Corrosion Crack Growth Rate and Strain Rate.

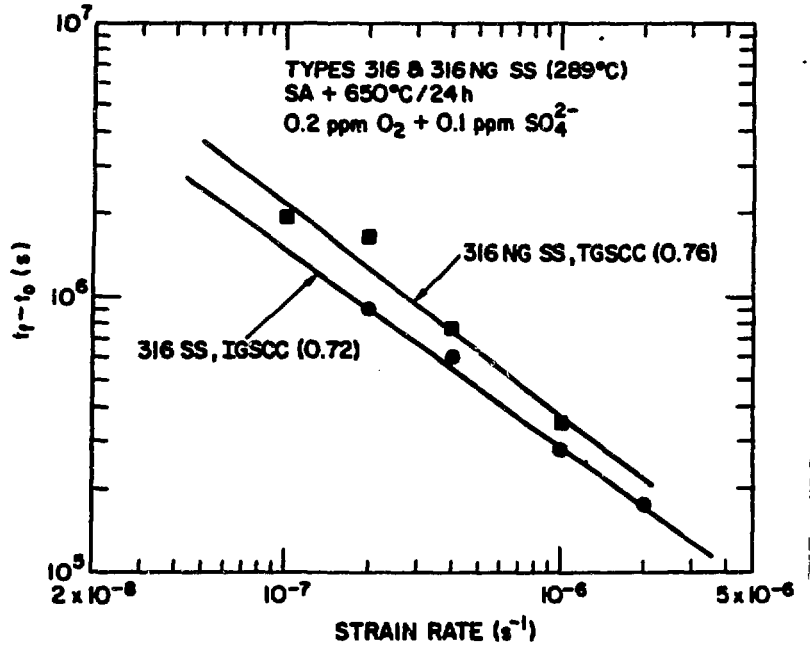

Fig. 6. Correlation between Time to Failure and Strain Rate for Failure by IGSCC and TGSCC.

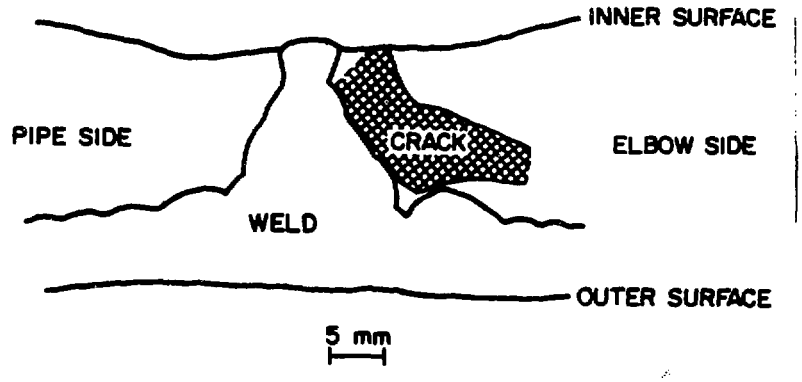

Fig. 7. Mapping of Axial Crack at 81-cm Position in Weldment C2.

Fig. 8. Crack Tip of Axial Crack at 81-cm Position in Weldment C2.

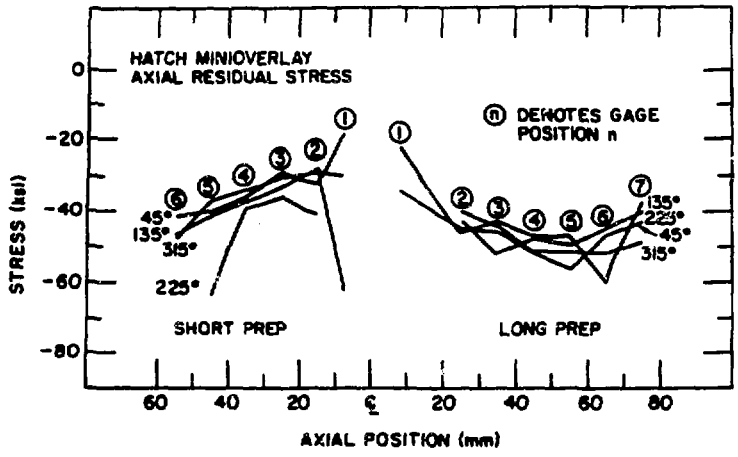

(a)

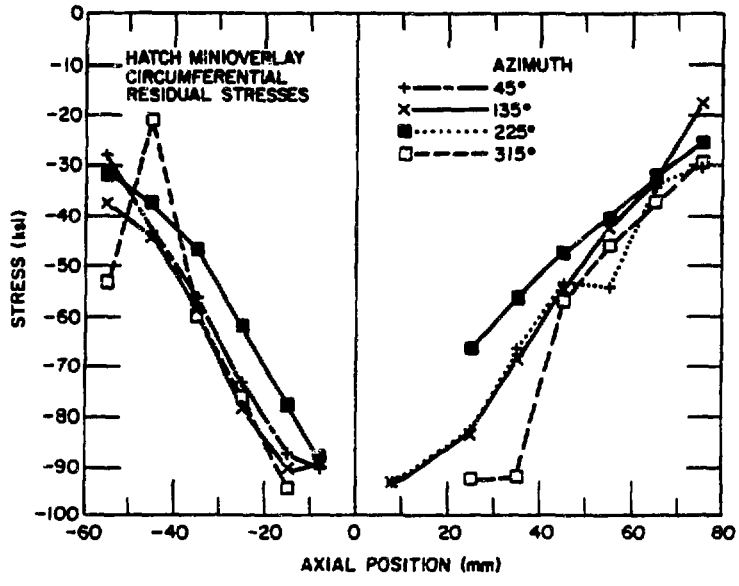

(b)

Fig. 9. (a) Axial and (b) Circumferential Residual Stresses on the Inner Surface at Four Azimuths of the Hatch Minioverlay Mock-up Weldment.

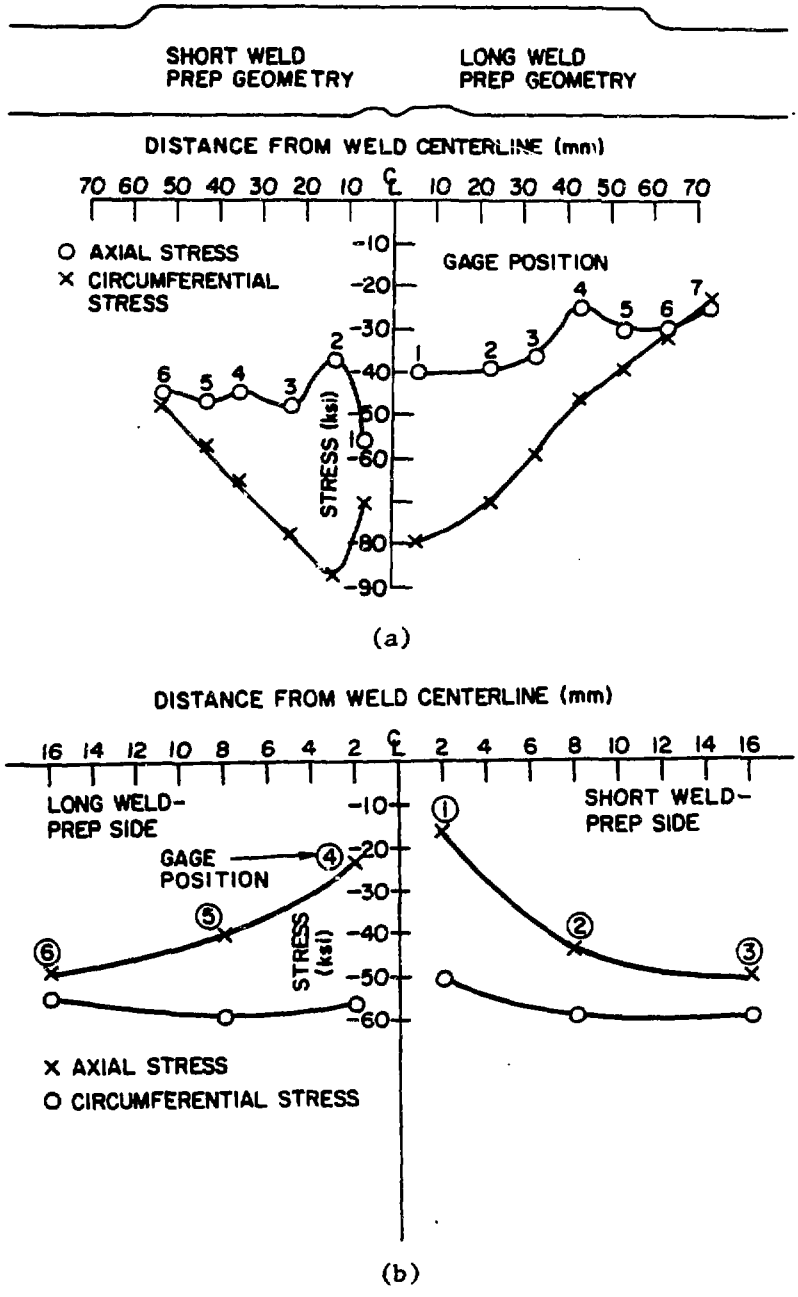

Fig. 10. Axial and Circumferential Residual Stresses on the Inner Surface of the Hatch (a) Standard Overlay Weldment and (b) LPHSW Mock-up Weldment.

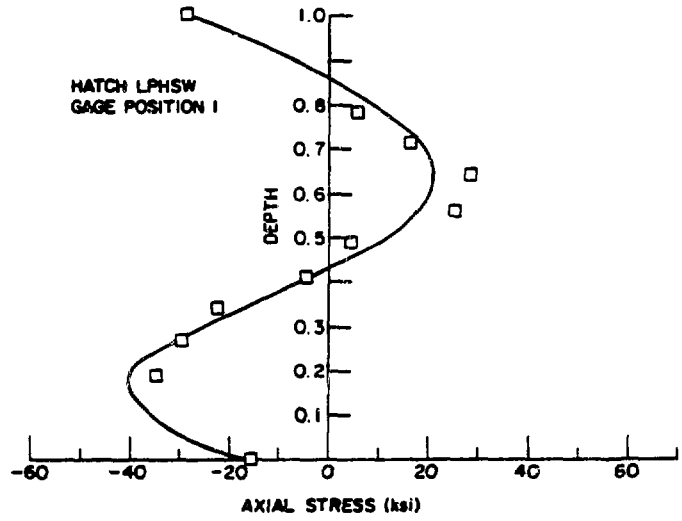

(a)

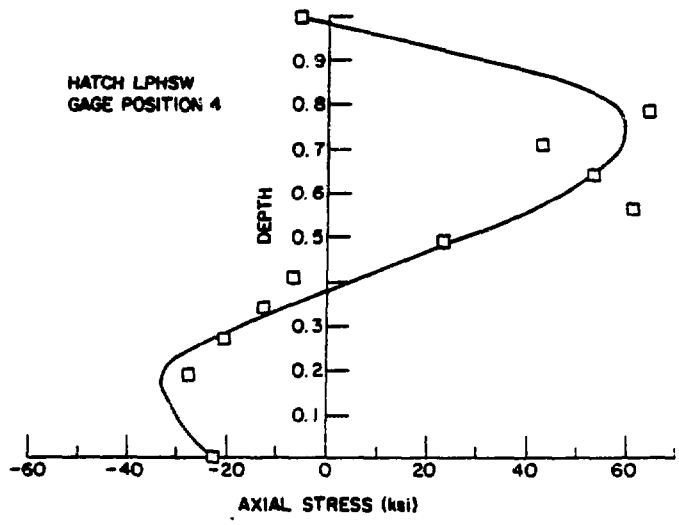

(b)

Fig. 11. Throughwall Axial Residual Stresses ∿2 mm from the WFL on (a) the Short Weld Prep Side and (b) the Long Weld Prep Side of the Hatch LPHSW Mock-up Weldment.

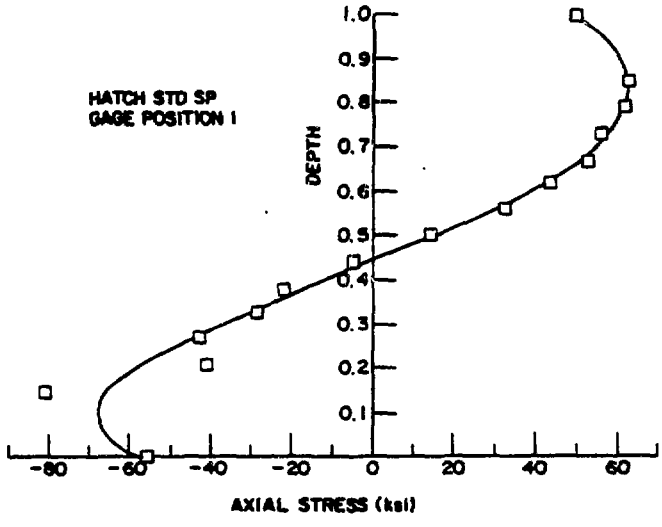

(a)

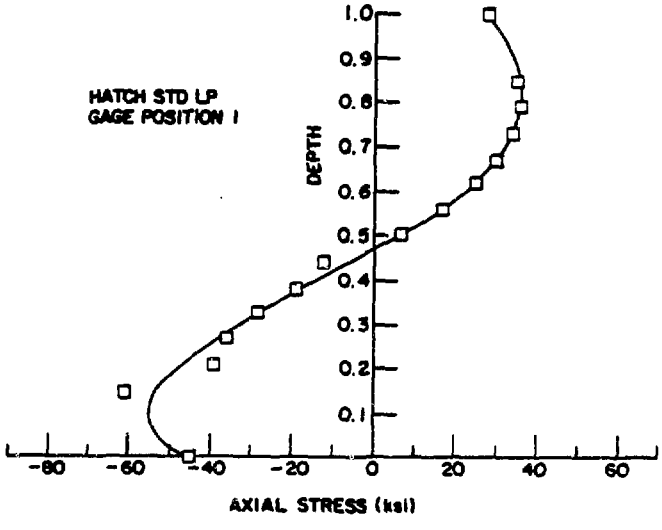

(b)

Fig. 12. Throughwall Axial Residual Stresses ∿2 mm from the WFL on (a) the Short Weld Prep Side and (b) the Long Weld Prep Side of the Hatch Standard Overlay Mock-up Weldment.

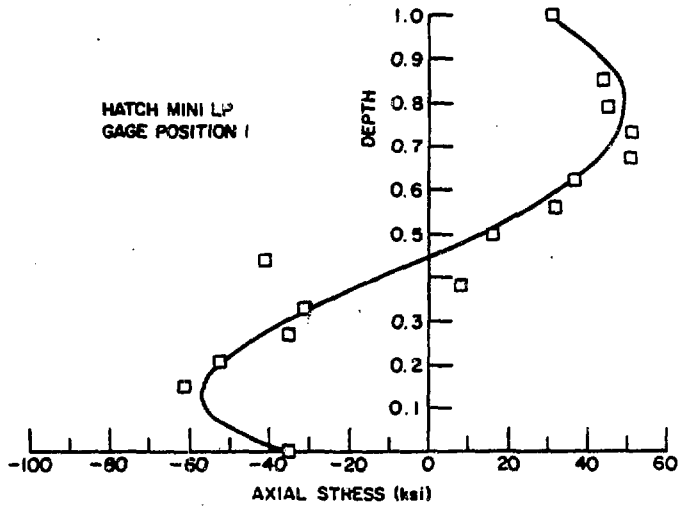

Fig. 13. Throughwall Axial Residual Stresses ∿2 mm from the WFL on the Long Weld Prep Side of the Hatch Minioverlay Mock-up Weldment.